Front. Med. 2025, 19(6): 1144−1162
https://doi.org/10.1007/s11684-025-1182-y

RESEARCH ARTICLE

ASPH interacts with RUVBL2 to promote tumor metastasis in lung adenocarcinoma via MAPK and Notch signaling pathways

Chuhong Huang[1], Huihao Lu[1], Jiali Dong[1], Yanming Lin[1], Yuting Chen[1], Zhixiong Yang[1], Wenmei Su (✉)[1,2], Zhen Cheng (✉)[1,2]

[1]Affiliated Hospital of Guangdong Medical University, Zhanjiang 524000, China; [2]Zhanjiang Key Laboratory of Tumor Microenvironment and Organoid Research, Zhanjiang 524000, China

Abstract **Aspartate/asparagine-β-hydroxylase (ASPH), a type II transmembrane α-ketoglutarate-dependent hydroxylase, is frequently overexpressed in various cancers. However, its role in lung adenocarcinoma (LUAD) remains unclear. Here, we analyzed ASPH expression in LUAD and normal lung tissues using bioinformatic tools, and evaluated its association with clinicopathological characteristics and patient prognosis. High ASPH expression correlated with advanced disease and poor survival, and served as an independent prognostic factor. Functional assays, including Transwell, scratch healing, and murine lung metastasis models, demonstrated that ASPH promotes LUAD cell migration and metastasis. The potential molecular mechanisms by which ASPH exerts its function in LUAD were explored by transcriptome sequencing analysis and immunoprecipitation combined with mass spectrometry (IP-MS). Further analysis showed that ASPH enhances activation of the MAPK and Notch signaling pathways through RUVBL2 interaction. Collectively, our findings suggest that ASPH contributes to LUAD progression by engaging RUVBL2 and activating key oncogenic signaling cascades, highlighting its potential as a prognostic biomarker and therapeutic target.**

Keywords ASPH; RUVBL2; MAPK signaling pathway; Notch signaling pathway; lung adenocarcinoma metastasis

Introduction

Lung cancer is a common malignant tumor worldwide and remains the leading cause of cancer-related deaths [1]. Currently, more than 85% of lung cancers are categorized as non-small cell lung cancer (NSCLC), mainly lung adenocarcinoma (LUAD) and lung squamous cell carcinoma (LUSC) [2]. The treatment modalities for early-stage lung cancer are mainly based on surgery, and with the development of therapies such as immunotherapy and targeted therapies, the survival time of patients has been prolonged and their quality of life has improved [3]. However, some patients are diagnosed only in the advanced stage of the disease, mostly accompanied by organ metastasis, losing the chance of surgery and having a low 5-year survival rate [4]. Therefore, identifying biomarkers for LUAD that can be used for early diagnosis and elucidating the molecular mechanisms of LUAD metastasis are important for improving patient prognosis and developing therapeutic targets.

Aspartyl/asparaginyl-β-hydroxylase (ASPH) is a type II transmembrane hydroxylase and a member of the highly conserved α-ketoglutarate-dependent hydroxylases family [5]. An increasing number of studies have found that ASPH expression is upregulated in a variety of tumor tissues and correlates with poor patient prognosis [6–13]. Previous studies have found that ASPH is highly expressed in LUAD; however, its biological role and specific molecular mechanisms are unknown [14]. In breast cancer, the ASPH-Notch axis has been reported to induce specific exosome production to promote multi-organ metastasis of the cancer [7]. In hepatocellular carcinoma, ASPH interacts with INPP5F, leading to nuclear ectopia of INPP5F and activation of Notch signaling to promote tumor growth in hepatocellular carcinoma cells [12]. Therefore, we hypothesized that ASPH may play a pro-cancer role in LUAD.

In this study, we aimed to explore the differences in the expression of ASPH in normal tissues and LUAD using bioinformatics methods and to analyze the correlation

Received March 31, 2025; accepted August 27, 2025

Correspondence: Zhen Cheng, chengzhen@gdmu.edu.cn;
Wenmei Su, suwenmei123@163.com

between the abnormal expression of *ASPH* and the clinicopathological characteristics of patients with LUAD and its correlation with survival prognosis. The biological role of ASPH in LUAD was explored *in vivo* and *in vitro* by cell and animal experiments, and mined by Kyoto Encyclopedia of Genes and Genomes (KEGG) enrichment analysis and gene set enrichment analysis (GSEA). ASPH may be involved in signaling pathways, and potential interactions with ASPH were investigated by immunoprecipitation-mass spectrometry (IP-MS), with the aim of revealing its molecular mechanism of action in LUAD development and progression, and to provide a theoretical basis for ASPH as a new prognostic marker and therapeutic target for LUAD.

Materials and methods

Clinical data

Ten patients with LUAD who underwent tumor resection at the lung tumor specialist of Guangdong Medical University from March 2023 to March 2024 were selected, including 6 males and 4 females, with a mean age of (71.58 ± 4.56). Inclusion criteria: all patients underwent tumor resection for LUAD, postoperative pathological examination revealed adenocarcinoma, and the tissue specimens were housed in the specimen bank of the Lung Tumor Specialist of Guangdong Medical University. Tumor tissues of the same size and corresponding paracancerous tissues were removed from the postoperative specimens of each patient, placed in labeled tissue freezing tubes, and tissue proteins were extracted by adding an equal amount of 1× RIPA lysis buffer for homogenization. The study was approved by the Ethics Committee of the Affiliated Hospital of Guangdong Medical University (Approval No. YJKT2025-030-1). Inform consent was obtained from each patient.

Public data access and analysis

Data access

We first downloaded the uniformly normalized ($\log_2(x+1)$) TCGA-LUAD gene expression RNA high-throughput sequencing dataset (n = 576) and patient clinical information data (n = 707) from the UCSC Xena database and clinical samples with gaps in clinical information to obtain 576 sample data with largely complete clinical information after RNA sequencing were used for subsequent gene expression and clinicopathological characterization. A total of 517 LUAD samples and 59 paracancerous normal tissue samples were obtained, including 311 females and 265 males.

ASPH expression data analysis

ASPH mRNA expression data of 59 paired LUAD tumor tissues and normal tissues adjacent to the cancer were analyzed using R software (version 4.3.2), and the ggpubr package was used to visualize the paired results. We used the UALCAN website to enter the CPTAC analysis page by selecting "Proteomics," entering the gene name "*ASPH*," and selecting "Lung adenocarcinoma." Enter the gene name "*ASPH*," select the "Lung adenocarcinoma" dataset, choose "Total-Protein," and download the box plots of differential protein expression of ASPH in LUAD. Box plots of ASPH protein expression differences in LUAD were downloaded and re-displayed with the P value (2.66×10^{-7}) shown on the website. ASPH expression in patients from different clinicopathological groups was extracted, and the data were visualized using GraphPad Prism 8.0 software.

Characterization of ASPH expression and clinicopathology

The data analysis of *ASPH* expression and clinicopathological characteristics in LUAD was performed using SPSS software (version 26.0), and the LUAD samples were classified into the high-expression group (n = 164) and low-expression group (n = 412) according to the upper 1/4 quartile of the expression value (75% threshold) of *ASPH* mRNA expression values. The information about the clinicopathological characteristics such as the patient' s age, sex, smoking history, T stage, N stage, M stage, clinical stage, survival status, were collected. By matching the sample number, the patient clinicopathological characteristics information corresponded to the *ASPH* expression values one by one. Clinicopathological characteristics were dichotomized by age (< 60 years vs. ⩾ 60 years), sex (female vs. male), smoking history (yes vs. no), T stage (T1 + T2 vs. T3 + T4), N stage (N0 vs. ⩾ N1), M stage (M0 vs. M1), clinical stage (Stage I + II vs. Stage III + IV), and survival status (living vs. deceased) were dichotomized, and the Pearson χ^2 test was used to compare the clinicopathological characteristics of the two groups of patients.

Cox proportional risk modeling of clinicopathologic features and ASPH expression with overall survival (OS) in LUAD

Clinical data of LUAD patients in the *ASPH* high-expression group and the data in the low-expression group were extracted, and the clinical characteristics such as age (years), sex, tumor diameter, clinical stage, T stage, N stage, M stage, survival status, and survival time were selected, according to age (< 60 vs. ⩾ 60 years), sex (male vs. female), clinical stage (Stage I + II vs. Stage

III + IV), tumor diameter was treated as a continuous variable, and regression analysis was performed using SPSS software (version 26.0), and the clinicopathological characteristics with statistically significant differences in the univariate regression analysis were subjected to multivariate regression analysis.

Survival prognosis analysis

The Kaplan–Meier Plotter database was used to obtain survival rates according to the Kaplan–Meier method, and the Log-rank test was used to compare survival curves. To open the online Kaplan–Meier plotter (Pan-cancer RNAseq, TCGA survival) [15], enter "*ASPH*" or "*RUVBL2*" in "Gene symbol", select "upper quartile" for "Split patients by", select "upper quartile" for "Survival" and select "Lung adenocarcinoma" for the dataset. LUAD (n = 513), and the remaining options were defaulted, and PDF images were exported and re-displayed.

Analysis of IP-MS results

We sorted the identified proteins in order of protein abundance from largest to smallest, and found that 201 identified proteins in the H1299-IgG group had an expression abundance of 0. We selected these 201 proteins as well as the proteins identified in the H1299-ASPH group with protein expression abundance sorted among the top 201 proteins for intersection analysis and the intersection resulted in 14 candidate proteins.

Enrichment analysis of the ASPH pathway

For KEGG enrichment analysis, we first divided the samples into a high *ASPH*-expressing gene group and a low *ASPH*-expressing gene group based on the median *ASPH* mRNA expression level, and the Limma package in R was used to analyze the genes of the two groups differentially and derive the differential results. Differentially expressed genes (DEGs) were screened, and the screening criteria were both $P < 0.01$, $|\log_2(FC)| > 1$, FC is the fold change, and the KEGG pathway was analyzed using the cluster-Profiler R package for DEGs. The cluster-Profiler R package was used for GSEA. The number of random combinations was set to 1000, the false discovery rate was FDR < 0.25 and $P < 0.05$, and the enrichment results were visualized using the ggplot2 package.

RT-qPCR

Tissue samples were removed from the specimen bank, and cancer tissues and their paired paracancerous tissue samples of the same volume and size were cut and added to well-labeled grinding tubes, with 2–3 grinding beads added to each tube. TRIzol reagent was added to each tube, the tissues were fully ground using a cryo-mill, and total RNA was extracted from the homogenate obtained. Reverse transcribe the total RNA (1 μg) to synthesize the template cDNA and analyze the expression of *ASPH* using *GADPH* as an internal reference, followed by a two-step PCR procedure according to the manufacturer's qPCR kit. The reaction conditions were set as follows: step 1 (pre-denaturation), 95 °C, 2 min, 1 cycle; step 2 (PCR reaction): 95 °C denaturation for 5 s, 60 °C annealing extension for 30 s, 40 cycles; and step 3 (solubility curve analysis), 60 °C, 15 s. Relative expression was expressed as $2^{-\triangle\triangle Ct}$. *ASPH* primer information: forward primer CTACGTGGAGCCATCG-AGAC; reverse primer ATCCCACGCCAAGGTCATTT. *RUVBL2* primer information: forward primer ATGGC-AACCGTTACAGCCA; reverse primer TGGGGCTACC-ATGGCATTTC.

Western blot

Cells were lysed on ice using a pre-formulated RIPA cell lysate + 1% protease inhibitor + 1% phosphatase inhibitor, and protein assays were performed using the bicinchoninic acid assay (BCA) method, with the addition of 20% volume of 5× loading buffer and an equal volume of purified water for experiments (30 ng/sample). Proteins were separated by sodium dodecyl sulfate-polyacrylamide gel electrophoresis (SDS-PAGE). Proteins were transferred to PVDF membranes using Tris-glycine solution. Protein membrane bands were cut according to the target molecule size and position indicated by the protein marker. Non-specific binding was blocked by addition of 5% skim milk powder at room temperature. The protein bands were washed with Tris-buffered saline with Tween (TBST) containing Tween-20 and incubated for 16–18 h at 4 °C with a protein primary antibody. The secondary antibody was added after washing with TBST and the membranes were incubated for 1 h at room temperature. The luminescent solution was added after washing with TBST and was placed in a colorimetric imager for development and photographic documentation.

Cell lines and culture

Human LUAD cell lines A549 and H1299 were purchased from Procell Life Science and Technology Co. Ltd (Procell, Wuhan, China). 293T cells were a generous gift from Dr. Gao Xiao's group at the Respiratory Research Institute of the Guangdong Medical University Hospital. Different cell lines were cultured using different types of media: A549 cells were cultured using F12K medium (Procell, Wuhan, China); H1299 cells were cultured using RPMI-1640 medium (Gibco); and 293T

cells were cultured using DMEM high glucose medium (Gibco). All cells were cultured at 37 °C and 5% CO_2 in a constant temperature incubator.

Lentivirus, siRNA, plasmid construction and cell transfection

To generate lentiviruses, we first inoculated 293T cells into 10 cm cell culture dishes and cultured them to 80% confluence. The cells were then transfected with 12 μg of plasmid DNA, 8 μg of Δ8.9, and 4 μg of vesicular stomatitis virus G glycoprotein (VSV-G) mixed with 40 μL of Lipofectamine 3000 and 50 μL of P3000 reagent (Invitrogen, Carlsbad, USA) in OPTI-MEM (Gibco). The medium was changed at 12 h after transfection. Supernatants containing lentivirus were collected at 48 and 72 h post-transfection and stored at −80 °C. Full-length human *ASPH* and sh-ASPH plasmids were selected and inserted into the pLVX-IRES-Puro vector for stable overexpression and knockdown, respectively. The empty plasmid Plenti-CMV-Lv105 was used as a control and Plenti-CMV-ASPH-Lv105 (EX-Z8758-Lv105) was used as the vector for ASPH. All stably expressing cells carried GFP, which produced green fluorescence. The siRNA sequence information was shown in Table S1.

ASPH overexpression plasmids and small interfering RNA were purchased from General Bio (Chuzhou, China). RUVBL2 small interfering RNA were purchased from GenePharma (Suzhou, China). Cells were transfected using the Lipofectamine 3000 kit (Invitrogen, Carlsbad, USA) according to the manufacturer's instructions.

Transwell experiments

Two hours before the start of the experiment, Transwell chambers were placed in 24-well plates and 100 μL of 1× matrix gel was added to the upper chamber of the invasion chambers. After 48 h of transfection with siRNA or overexpression plasmid, the cells were digested, centrifuged, resuspended in serum-free medium, and counted. 100 μL of serum-free medium containing 25 000 cells was added to the top of the chambers, and 600 μL of complete medium containing 10% fetal bovine serum was added to the bottom of the chambers, and the cells were placed in the migration incubator for 12–16 h. The migration experiment did not require the addition of matrix gel. The Transwell was removed, the medium was discarded, the cells were washed once with PBS, and fixed with methanol for 20 min. The methanol was discarded, washed once with PBS, stained with 0.1% crystal violet for 20 min, recovered, and washed with pure water. The upper layer of non-migrated cells was gently wiped off using a cotton swab and air-dried. Randomly selected fields of view were observed under a microscope and photographed.

Scratch healing experiment

Cells were inoculated in 6-well plates and after transfection, when the cell density reached 100%, a scratch operation was performed, the original medium was discarded, and the cells were rinsed with PBS buffer for 2 times, A549 was added to serum-free medium to continue cultivation, and H1299 was added to 3% FBS medium. Scratch healing was observed and recorded at 0 h and 24 h. The scratch area was analyzed using ImageJ software, and the scratch healing rate (%) was calculated as (scratch area at 0 h − scratch area at 24 h)/scratch area at 0 h × 100%.

PD0325901 and DAPT experiments

H1299 cells were cocultured with Mirdametinib (as known as PD0325901, 10 μmol/L; a well-known MEK/ERK pathway inhibitor for MAPK, MCE, HY-10254, Shanghai, China) or DAPT (10 μmol/L; a well-known γ-secretase inhibitor for Notch, MCE, HY-13027, Shanghai, China) for 24 h after transfection with a negative control or ASPH plasmid. Transwell assay, scratch healing assay and Western blot were performed as described above.

CCK-8 experiment

Add 100 μL of cell suspension containing 1000 cells transfected with NC, siRNA, or overexpression plasmid into 96-well plates, set up five replicate wells, add PBS around the 96-well plate, remove the medium at fixed time points and add 100 μL of medium containing 10% CCK-8 reagent. After 2 h of incubation in the incubator, the absorbance (OD) value at 450 nm was measured using an enzyme meter for 4 consecutive days. Graphs were analyzed using GraphPad Prism software (version 8.0) to determine the differences in cell growth and proliferation and draw growth curves.

Clone formation experiments

After transfection with siRNA or overexpression of plasmid for 48 h, 200 cells were inoculated into 6-well plates with 10% FBS medium and placed in a cell culture incubator for 14 d. Cells were fixed with methanol and stained with 1% crystal violet.

IP-MS

Cells were washed twice with ice-cold PBS and lysed

with immunoprecipitation lysis buffer (PC101, Epizyme, Shanghai, China) containing protease and phosphatase inhibitors (CoWin Biosciences, Jiangsu, China) for 15 min on ice. The lysate was collected and pre-purified with Pierce A/G protein magnetic beads (YJ003, Epizyme, Shanghai, China) with 10% lysate as the input. Cell lysates were immunoprecipitated with 1 μg of the relevant antibody at 4 °C overnight. The antibodies used for immunoprecipitation were as follows: ASPH (ab172475, Abcam), RUVBL2 (10195-1-AP, Proteintech), and IgG antibody (30000-0-AP, Proteintech) were used as negative controls. The immune complexes were incubated with Protein A/G magnetic beads for 4 h at 4 °C. The magnetic beads were separated using a magnetic separation stand and the supernatant was discarded. The magnetic beads were washed five times with immunoprecipitation lysis buffer, loading buffer diluted with immunoprecipitation RIPA buffer was added, and protein denaturation was carried out in a metal bath at 98 °C for 10 min. Protein immunoblotting experiments were carried out using SDS-PAGE gels, or the samples were sent to BGI Genomics Co., Ltd. (Shenzhen, China) for protein profiling.

Construction of pulmonary metastasis model in murine caudal vein

The animal experiments in this study were approved by the Animal Experimentation Ethics Committee of the Affiliated Hospital of Guangdong Medical University (approval no. AHGDMU-LAC-B-2023-11-0017). The experimental animals were BALB/c nude female rats, purchased from Guangzhou Chase Ruihua Biotechnology Co. Ltd., at 4–6 weeks of age, with a license for the use of experimental animals (SYXK(GD) 2022-0286). The nude mice were kept in an SPF-grade sterile environment, and bedding and feed were provided by the Experimental Animal Center of the Affiliated Hospital of Guangdong Medical University. To construct a murine tail vein lung metastasis model, we injected 1 × 106 A549 cells with stable low ASPH expression into the tail vein of nude mice. All mice were sacrificed after 10 weeks, and lung tissues were dissected and fixed using Bouin's fixative. Lung tissues were observed, photographed, and dehydrated using a fully automated dehydrator for subsequent hematoxylin and eosin (HE) staining and immunohistochemical analysis.

Immunohistochemistry (IHC) and HE staining

Paraffin-embedded lung tissues were sliced at a thickness of 5 μm and baked at 60 °C for 2 h. After deparaffinization with xylene and rehydration with a range of ethanol concentrations, slides were boiled in 1× EDTA antigen repair solution (BL618A, Biosharp, Beijing, China) for antigen recovery, and non-specific binding was blocked with 20% goat serum. Primary antibodies for Notch1 (Proteintech, 20687-1-AP, dilution 1:100) and p-ERK (Cell Signaling Technology, 4370T, dilution 1:50) diluted in PBS were then added and incubated overnight in a refrigerator at 4 °C. After rinsing three times in PBS, the sections were incubated with secondary antibodies, rinsed three times with PBS, and incubated with the secondary antibody for 30 min, and then the results were detected using a 3,3′-diaminobenzidine (DAB) peroxidase substrate kit (G1212-200T, Servicebio, Hubei, China). For HE staining, the slides were stained with HE after deparaffinization and rehydration.

Statistical analysis

Correlation analysis of ASPH expression with clinicopathological characteristics and COX proportional risk analysis were performed using SPSS software (version 26.0). The experimental data were statistically analyzed using GraphPad Software 8.0. Comparison of data between two groups was performed using the *t*-test, and comparison of data above two groups was statistically analyzed using one-way ANOVA. All data are expressed as mean ± standard deviation (SD). $P > 0.05$ was considered statistically significant (ns) and $P < 0.05$ was considered statistically significant.

Results

ASPH is highly expressed in LUAD

By analyzing the high-throughput sequencing data of cancer and paracancerous tissues of 59 paired cases of LUAD from the The Cancer Genome Atlas (TCGA) database, it was found that *ASPH* mRNA expression was significantly higher in tumor tissues than in normal tissues, and the difference was statistically significant between the two groups ($P < 0.001$, Fig. 1A). Protein expression analysis of cancer and para-cancer tissues of 111 LUAD patients using the protein expression database CPTAC showed that ASPH protein expression was significantly higher in tumor tissues than in normal tissues, and the difference was statistically significant ($P < 0.001$, Fig. 1B). We further analyzed the relationship between ASPH expression and different tumor stages, and found that patients with advanced LUAD (Stage III + IV) had significantly higher *ASPH* mRNA expression than patients with early-stage (Stage I + II), and the difference between the two groups was statistically significant ($P < 0.05$, Fig. 1C); compared to LUAD patients with smaller tumor diameters (T1 and T2), the expression of *ASPH* mRNA was significantly higher in the LUAD tissues of patients with larger tumor diameters

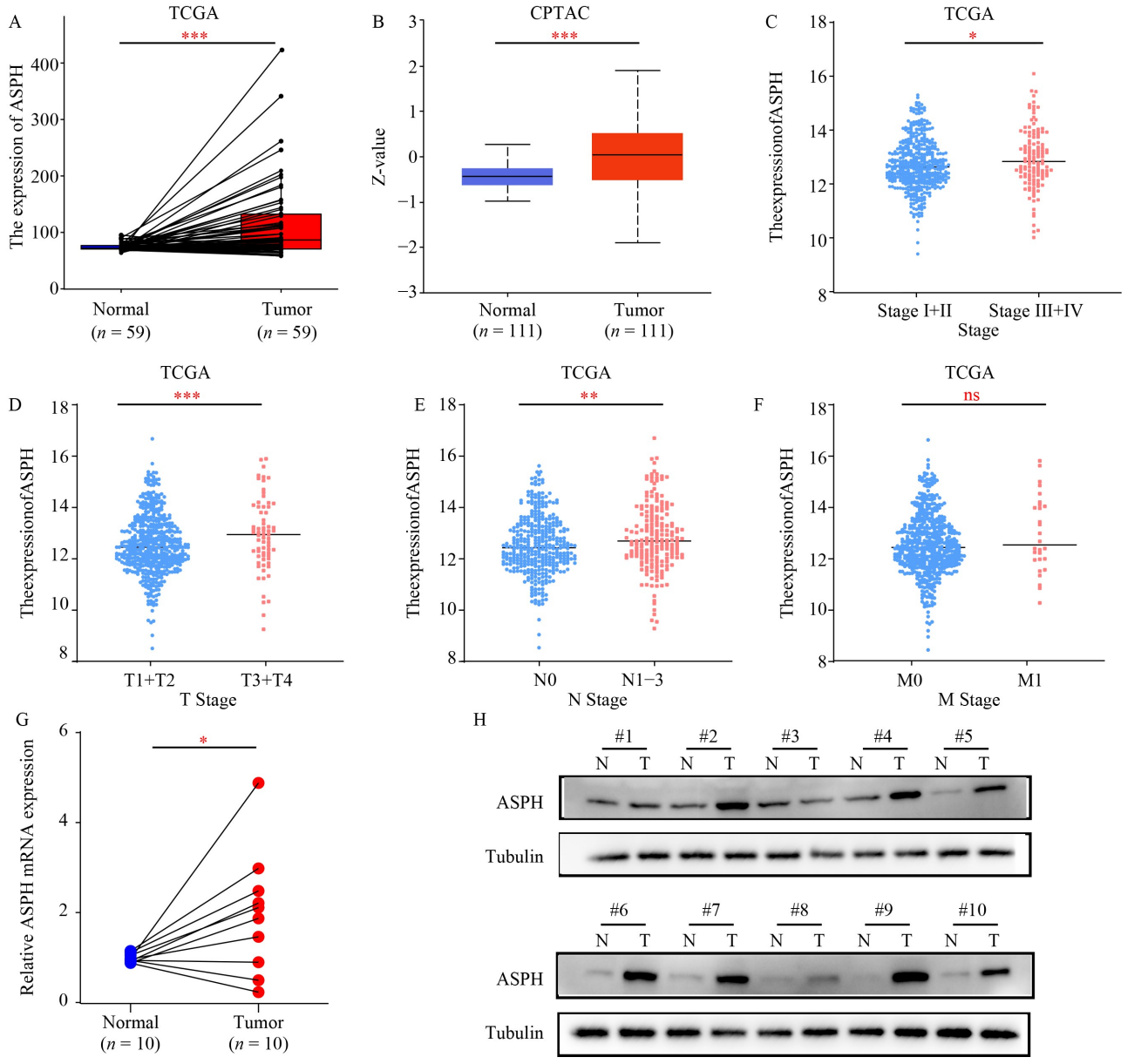

Fig. 1 ASPH is highly expressed in LUAD. (A) High-throughput sequencing analysis of 59 paired cancer and para-cancer tissues of LUAD in TCGA database, *ASPH* mRNA expression in LUAD tissues and para-cancer normal tissue. (B) Protein sequencing results of 111 paired cancer and para-cancer tissues of LUAD from CPTAC database, ASPH protein expression in LUAD tissues and paracancerous normal tissues. (C–F) *ASPH* mRNA expression in LUAD patients with different (C) clinicopathological stages, (D) T stage, (E) N stage and (F) M stage from the TCGA database. (G) RT-qPCR analysis of *ASPH* expression in 10 paired LUAD tissues and paraneoplastic tissues. (H) Protein immunoblotting experiments to analyze ASPH expression in 10 paired LUAD tissues and paraneoplastic tissues. ns, not statistically significant, *$P < 0.05$, **$P < 0.01$, ***$P < 0.001$. TCGA, The Cancer Genome Atlas; CPTAC, Clinical Proteomic Tumor Analysis Consortium; ASPH, aspartate β-hydroxylase; N, normal; T, tumor.

(T3 and T4), and the difference was statistically significant ($P < 0.001$, Fig. 1D); compared with LUAD patients without lymph node metastasis (N0), *ASPH* mRNA was more highly expressed in LUAD tissues of patients with developed lymph node metastasis (N1–N3), and the difference was statistically significant ($P < 0.01$, Fig. 1E); compared with LUAD patients without distant metastasis (M0), *ASPH* mRNA was more highly expressed in LUAD tissues of patients who had developed distant metastasis (M1), but the difference was not statistically significant ($P > 0.05$, Fig. 1F), and it was considered that this result might be related to the smaller number of samples from patients who had developed distant metastasis (M1).

To further verify the specific expression of ASPH in LUAD tissues, we collected tumor tissues and

corresponding para-carcinoma tissues from 10 LUAD patients attending our hospital, and detected the expression by RT-qPCR and protein blotting experiments. The RT-qPCR results revealed that *ASPH* mRNA was higher in LUAD tissues compared with para-carcinoma tissues, and the difference was statistically significant ($P < 0.001$, Fig. 1G), consistent with the previous bioinformatics analysis. Protein immunoblotting results revealed that the protein expression level of ASPH was significantly higher in LUAD tissues than in paracancerous lung tissues (Fig. 1H).

ASPH expression correlates with clinicopathologic characteristics

We explored the correlation between *ASPH* expression and clinicopathological characteristics by joint analysis of RNA sequencing data and patient clinical information data. The analysis results showed that high ASPH expression was significantly correlated with lymph node metastasis (N stage ⩾ N1), distant metastasis (M stage = M1), clinicopathological stage (stage III + IV) and patients' survival status, and the difference between the two groups was statistically significant ($P < 0.05$, Table 1).

ASPH expression is associated with poor prognosis in LUAD

The results of the analysis of *ASPH* expression and patients' OS and relapse free survival (RFS) are shown in Fig. 2A and 2B. Compared with the patients in the *ASPH* low-expression group, the *ASPH* high-expression group was shorter, and the *ASPH* expression was significantly and positively correlated with patients' poor prognosis (HR 1.85, 95% CI 1.38–2.48; HR 1.53, 95% CI 1.01–2.33; $P < 0.001$). In patients with advanced LUAD, OS was also shorter in the *ASPH* high-expression group, and the difference was statistically significant (HR 2.22, 95% CI 1.28–3.85; $P < 0.005$, Fig. 2C). RFS was also shorter in LUAD patients with advanced LUAD (stage III + IV) in the *ASPH* high-expression group of LUAD patients, but the difference between the two groups was not statistically significant ($P > 0.05$, Fig. 2D), and it was

Table 1 Relationship between *ASPH* expression and clinicopathologic features in the LUAD dataset of the TCGA database

Categories	Low *ASPH* expression patients ($n = 412$)	High *ASPH* expression patients ($n = 164$)	χ^2 value	*P* value
Age (year), *n* (%)			0.575	0.256
< 60	106 (26.6)	46 (29.7)		
⩾ 60	203 (73.4)	111 (70.3)		
Gender, *n* (%)			1.472	0.131
Female	229 (55.6)	82 (50.0)		
Male	183 (44.4)	82 (50.0)		
Smoking history, *n* (%)			0.036	0.494
Never	26 (14.9)	12 (15.8)		
Ever	149 (85.1)	64 (84.9)		
T stage, *n* (%)			3.286	0.050
T1 + T2	367 (89.5)	137 (84.0)		
T3 + T4	43 (10.5)	26 (16.0)		
N stage, *n* (%)			3.082	**0.049**
N0	276 (67.5)	98 (59.8)		
⩾ N1	133 (32.5)	66 (40.2)		
M stage, *n* (%)			3.498	0.053
M0	395 (96.3)	152 (92.7)		
M1	15 (3.7)	12 (7.3)		
Stage, *n* (%)			3.241	**0.047**
I + II	329 (80.0)	120 (73.2)		
III + IV	82 (20.0)	44 (26.8)		
Vital status, *n* (%)			5.583	**0.012**
Alive	272 (66.0)	91 (55.5)		
Deceased	140 (34.0)	73 (45.5)		

ASPH, aspartate β-hydroxylase; T, tumor; N, node; M, metastasis. Bolded font indicates statistically significant difference.

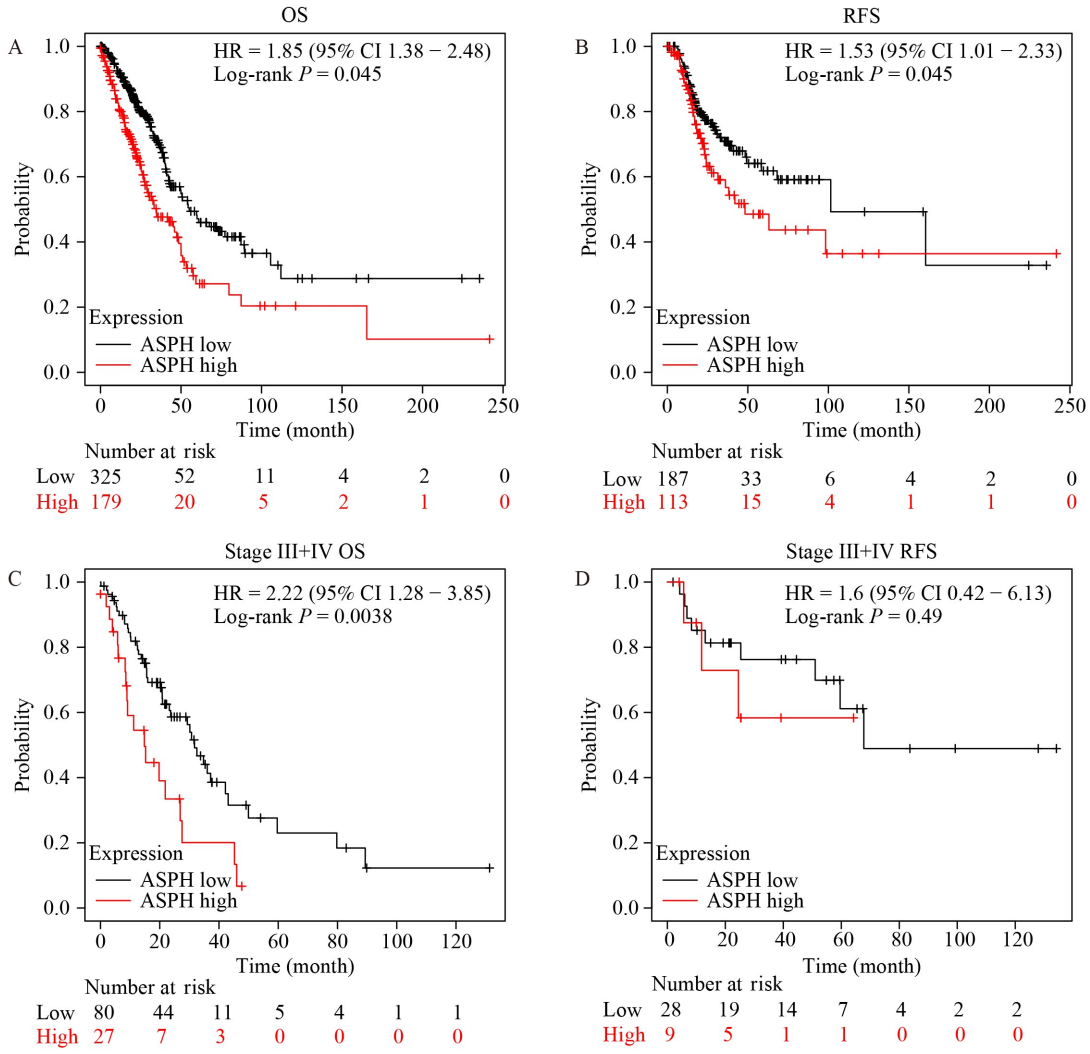

Fig. 2 *ASPH* expression is associated with poor prognosis in LUAD. (A, B) Kaplan–Meier survival curve analysis based on *ASPH* expression and OS and RFS of LUAD tissues. (C, D) Kaplan–Meier survival curve analysis based on *ASPH* expression and OS and RFS of LUAD tissues with pathologic stage III and IV. OS, overall survival; RFS, relapse free survival; ASPH, aspartate β-hydroxylase; HR, hazard ratio.

considered that it might be related to the clinical sample size was too small.

To clarify the prognostic factors affecting LUAD, we performed a univariate analysis of clinicopathological characteristic information, and found that: high expression of *ASPH* (HR = 1.52 (1.141–2.025), P = 0.004), advanced clinicopathological staging (HR = 2.63 (1.975–3.509), $P < 0.001$), tumor size (T stage, HR = 2.31 (1.606–3.318), $P < 0.001$), lymphatic metastasis (N stage, HR = 2.72 (2.068–3.58), $P < 0.001$), distant metastasis (M stage, HR = 2.14 (1.299–3.516), $P = 0.003$) were all positively associated with poor prognosis of LUAD and could be used as prognostic risk factors for LUAD (Table 2). High expression of *ASPH* (HR = 1.43 (1.067–1.913), P = 0.017), tumor size (HR = 1.64 (1.089–2.464), P = 0.018), and lymph node metastasis (HR = 2.31 (1.672–3.191), $P < 0.001$) were confirmed as independent prognostic factors by multifactorial analysis (Table 3).

ASPH promotes migration and invasion of LUAD cells

To clarify the effect of ASPH on the biological function of LUAD cells and to construct a cell model with corresponding ASPH expression, we first detected the expression of ASPH in two LUAD cell lines, A549 and H1299, by protein immunoblotting assay. The results showed that ASPH expression was relatively high in A549 cell line and relatively low in H1299 cell line (Fig. 3A). Therefore, we decided to knockdown the expression of *ASPH* gene by transfection of siRNA in A549 cell line, and transfect the overexpression plasmid to construct ASPH overexpression cell line in H1299 cell line. The RNA and protein of the cells were extracted at 48 and 72 h after transfection, respectively, and RT-qPCR

Table 2 Univariable COX regression analysis of clinicopathologic characteristics and OS rate in patients with LUAD

Variable	HR	95% CI	*P* value
Age	1.03	0.759–1.399	0.85
Gender (female vs. male)	1.12	0.851–1.466	0.425
Smoking history (never vs. ever)	0.82	0.486–1.365	0.437
Longest dimension	1.11	0.822–1.494	0.5
Clinic stage (I + II vs. III + IV)	2.63	1.975–3.509	**< 0.001**
T stage (T1 + T2 vs. T3 + T4)	2.31	1.606–3.318	**< 0.001**
N stage (N0 vs. ⩾ N1)	2.72	2.068–3.58	**< 0.001**
M stage (M0 vs. M1)	2.14	1.299–3.516	**0.003**
ASPH expression (low vs. high)	1.52	1.141–2.025	**0.004**

ASPH, aspartate β-hydroxylase; HR, hazard ratio; CI, confidence interval. T, tumor; N, node; M, metastasis. Bolded font indicates statistically significant difference.

Table 3 Multivariable COX regression analysis of clinicopathologic characteristics and OS rate in patients with LUAD

Variable	HR	95% CI	*P* value
Clinical stage (I + II vs. III + IV)	1.28	0.850–1.916	0.239
T stage (T1 + T2 vs. T3 + T4)	1.64	1.089–2.464	**0.018**
N stage (N0 vs. ⩾ N1)	2.31	1.672–3.191	< **0.001**
M stage (M0 vs. M1)	1.39	0.876–2.461	0.258
ASPH expression (low vs. high)	1.43	1.067–1.913	**0.017**

ASPH, aspartate β-hydroxylase; HR, hazard ratio; CI, confidence interval; T, tumor; N, node; M, metastasis. Bolded font indicates statistically significant difference.

and Western blot were applied to detect the transfection efficiency of ASPH. As shown in Fig. 3B and 3C, in A549 cell line, both siASPH-1 and siASPH-2 sequences significantly reduced the expression level of ASPH compared with the NC group, and the difference was statistically significant ($P < 0.001$); in H1299 cell line, overexpression of ASPH significantly increased the mRNA and protein expression levels compared with the vector, and the difference between two groups was statistically significant ($P < 0.001$), which indicated that the construction of the cell model of knocking down or overexpression of *ASPH* was successful, and could be used for the next biological function experiments.

To explore whether ASPH affects the migration and invasion ability of LUAD cells, we performed Transwell and scratch healing experiments. Results of Transwell experiments showed that the migration and invasion ability of cells were significantly decreased after knockdown of *ASPH* compared with the NC group ($P < 0.001$, Fig. 3D). While the migration and invasion ability of cells after overexpression of *ASPH* was significantly increased, and the difference was statistically significant ($P < 0.001$, Fig. 3E). The scratch healing assay showed that compared with the NC group, A549 cells in the knockdown *ASPH* group showed a decrease in scratch healing area after 24 h, and the difference between the two groups was statistically significant ($P < 0.001$, Fig. 3F); whereas compared with the Vector group, H1299 cells in the overexpression *ASPH* group showed an increase in scratch healing area after 24 h, and the difference between the two groups was statistically significant ($P < 0.001$, Fig. 3G).

To investigate whether ASPH affects the proliferative capacity of LUAD cells, we assessed the changes in proliferative capacity of LUAD cells after knockdown or overexpression of *ASPH* by CCK-8 and clone formation assays. As shown in Fig. 3H and 3I, in A549 cells, there was no significant change in the proliferative ability of cells after knockdown of *ASPH* compared with the NC group ($P > 0.05$); consistently, in H1299 cells, there was also no significant difference in the proliferative ability of cells between *ASPH* overexpression group and blank control group ($P > 0.05$). The results of clone formation experiments are shown in Fig. 3J and 3K, in A549 cells, there was no significant difference in the clone formation ability of cells between the siASPH-1 and siASPH-2 groups and the NC group ($P > 0.05$); similarly, in H1299 cells, there was no significant difference in the clone formation ability of cells between overexpression of *ASPH* group and the control group ($P > 0.05$).

The above results indicated that ASPH could promote the migration and invasion function of LUAD cells, but did not affect the cell proliferation function.

ASPH activates MAPK and Notch signaling pathways

After determining that ASPH affects the biological behavior of LUAD migration and invasion, this study

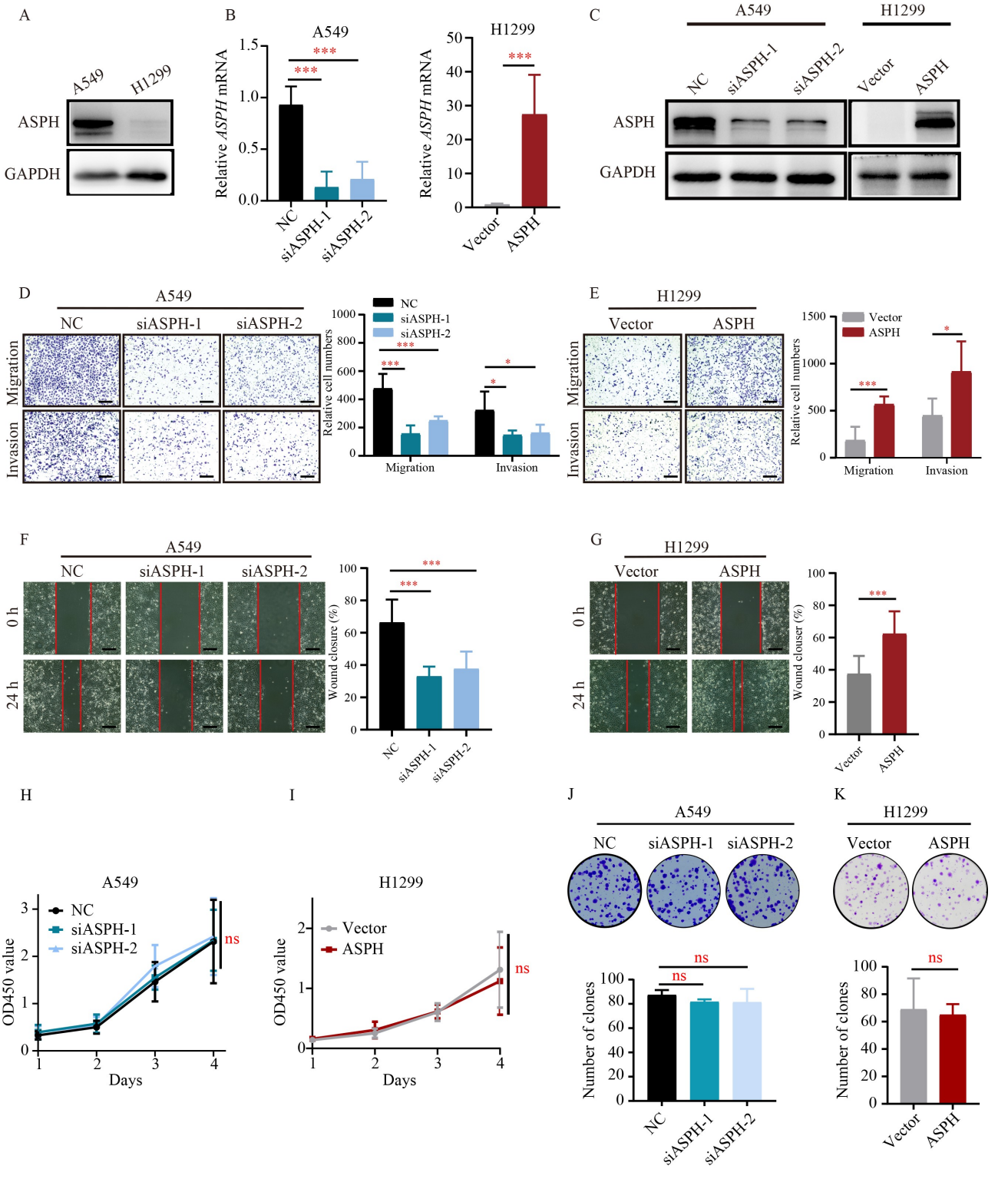

Fig. 3 ASPH promotes migration and invasion of LUAD. (A) Western blot assay to detect ASPH expression in LUAD cell lines A549 and H1299. (B, C) RT-qPCR and Western blot assays to detect the knockdown efficiency of *ASPH* in LUAD cell line A549 cells and overexpression efficiency of *ASPH* in H1299 cells, respectively. (D, E) Transwell assay to detect the effect of knockdown or overexpression of *ASPH* on the migration of A549 cells or H1299 cells. Scale bars = 200 μm. (F, G) Scratch healing assay to detect the effect of knockdown or overexpression of *ASPH* on migration and invasion of A549 or H1299 cells. Scale bars = 200 μm. (H, I) CCK-8 assay to detect the effect of knockdown or overexpression of *ASPH* on the proliferative capacity of A549 or H1299 cells. (J, K) Clone formation assay to detect the effect of knockdown or overexpression of *ASPH* on the clone formation ability of A549 cells or H1299 cells. **P* < 0.05; ****P* < 0.001; ns, not statistically significant. ASPH, aspartate β-hydroxylase.

further analyzed the intrinsic mechanism by which it affects the biological behavior of LUAD cells. We first divided the genes of *ASPH* mRNA in the high throughput sequencing data of LUAD from the TCGA database into ASPH high expression group and ASPH low expression group according to the median expression value (50% threshold), and analyzed the genes with differential expression using the Limma package in R, and the results of the differential analysis were shown as volcano plots (Fig. 4A). Subsequently, we defined the genes with expression difference folds greater than 1-fold and statistically significant differences as differential genes. KEGG pathway enrichment analysis of differential genes revealed that ASPH-related differential genes were enriched in the MAPK signaling pathway and PI3K-Akt signaling pathway (Fig. 4B). We further performed GSEA of differential genes based on KEGG pathway and found that ASPH was significantly positively enriched in MAPK signaling pathway (NES = 1.27, $P = 0.028$) and PI3K-Akt signaling pathway (NES = 1.08, $P = 0.284$) (Fig. 4C and 4D). Since previous studies have reported that ASPH plays an important role in the malignant process of other tumors by activating the Notch signaling pathway. We also performed GSEA on the Notch signaling pathway and found that ASPH differential genes were also significantly enriched in the Notch signaling pathway (Fig. 4E).

Next, we verified the effect of ASPH expression on the signaling pathway by Western blot. As shown in Fig. 4F, the phosphorylation levels of MEK and ERK, the key molecules of the MAPK signaling pathway, were significantly reduced by knocking down *ASPH*, and the expression of Notch1 was significantly downregulated, whereas there was no significant alteration in the phosphorylation levels of Akt and mTOR molecules. In H1299 cells, the phosphorylation levels of MEK and ERK proteins were significantly increased after overexpression of ASPH, and the expression of Notch1 was also significantly upregulated, but the phosphorylation levels of Akt and mTOR molecules were not significantly changed (Fig. 4G).

To further validate that ASPH promotes the development of LUAD by activating the MAPK and Notch signaling pathways, we conducted functional rescue experiments using the MEK/ERK inhibitor PD0325901 (PD03, 10 μmol/L) and the Notch inhibitor DAPT (10 μmol/L). As shown in Fig. 4H–4I and 4L–4N, compared to the ASPH-overexpressing group, the migration, invasion, and wound healing abilities of LUAD cells H1299 in the PD03 or DAPT treatment groups were significantly reduced ($P < 0.005$). Following treatment with PD0325901 or DAPT, ERK protein phosphorylation was reduced, and Notch protein expression levels decreased (Fig. 4J and 4K).

These results suggest that ASPH may promote the malignant process of LUAD through MAPK and Notch signaling pathways.

ASPH interacts with RUVBL2

Proteins are the main performers of cellular functions, and the study of protein-protein interactions (PPIs) is of great significance in understanding intracellular biological processes and revealing disease mechanisms. Therefore, in order to further explore the molecular mechanism of ASPH's role in LUAD, we proposed to search for proteins with potential possible interactions with ASPH by IP-MS. As shown in Fig. 5A, we successfully constructed a stable overexpression of ASPH in LUAD H1299 cell line that could be used for IP experiments. The results of mass spectrometry analysis showed that 3655 peptides and 601 proteins were identified in the H1299-IgG group, while 6561 peptides and 1064 proteins were identified in the H1299-ASPH group (Fig. 5B). The results are shown in Fig. 5C, by mass spectrometry analysis, we could obtain a total of 14 differentially expressed proteins that were highly expressed in the H1299-ASPH group but not in the H1299-IgG group, which were RUVBL2, LRRC59, HERC5, TUBA1B, RPL9, SPATS2L, EIF4A1, STAU2, RPL32, DHX30, DYNC1H1, NOP2, RPS15A, and HNRNPDL. We reviewed the literature related to these 14 differential proteins and found that RUVBL2 has been reported to be closely associated with the activation of the MAPK signaling pathway in colon cancer, but there are few reports on the expression and mechanism of action of RUVBL2 in LUAD. Therefore, we hypothesized that there might be an interaction between RUVBL2 protein and ASPH protein. We demonstrated the protein binding of ASPH protein to RUVBL2 by co-IP experiments: as shown in Fig. 5D, in H1299 cells stably expressing ASPH, the anti-RUVBL2 group antibody significantly enriched ASPH protein compared with the control group; consistently, the anti-ASPH group antibody also significantly enriched RUVBL2 protein.

Next, we detected the expression of RUVBL2 in LUAD A549 and H1299 cells through Western blot experiment. The results showed that there was no significant difference in the expression of RUVBL2 in these two cell lines (Fig. 5E). Then, we designed siRNAs targeting RUVBL2 (siRUVBL2-1 and siRUVBL2-2) and transfected them into A549 and H1299 cells. Then efficiency of *RUVBL2* mRNA and protein knockdown was verified by RT-qPCR and Western blot experiments. RT-qPCR results showed that, compared with the negative control group, *RUVBL2* mRNA expression levels were significantly reduced in the siRUVBL2-1 and siRUVBL2-2 groups, with statistically significant differences ($P < 0.001$, Fig. 5F and 5G). Western blot assay results showed that, compared with siNC group,

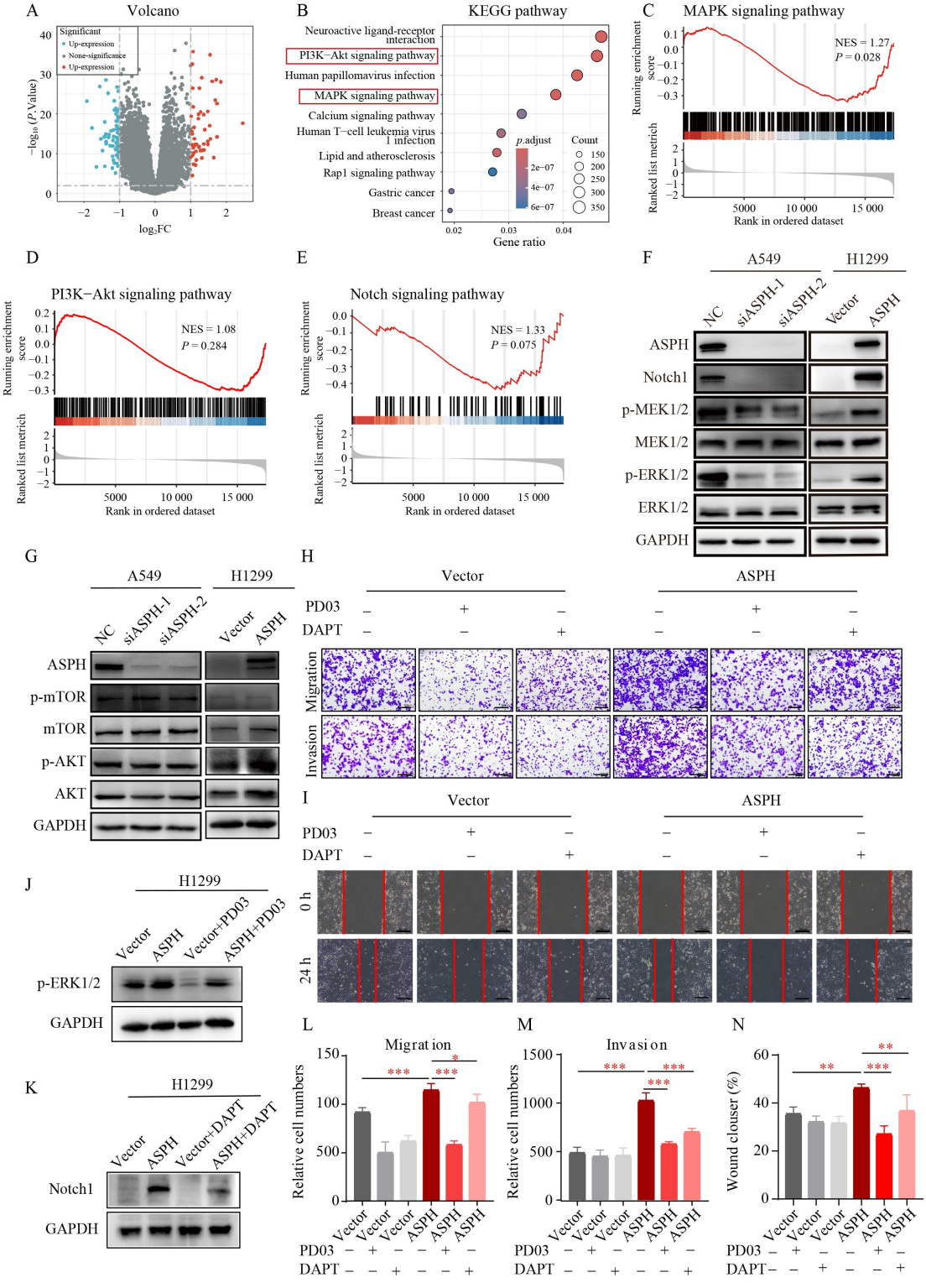

Fig. 4 ASPH activates MAPK and Notch signaling pathways. (A) Volcano plot of the results of *ASPH* gene-related differential analysis of TCGA-LUAD high-throughput sequencing data. (B) KEGG pathway enrichment analysis of ASPH-associated DEGs. (C–E) Results of GSEA of ASPH-associated differential genes in the MAPK signaling pathway, the PI3K-Akt signaling pathway, and the Notch signaling pathway. (F) The effects of knockdown or overexpression of *ASPH* on MAPK signaling pathway and Notch signaling pathway on LUAD cell lines A549 or H1299 cells. (G) Effects of knockdown or overexpression of *ASPH* on PI3K-Akt signaling pathway on LUAD cell lines A549 or H1299 cells. (H–N) After treatment with MEK/ERK inhibitor PD0325901 or Notch inhibitor DAPT (10 μmol/L), the migration, invasion, and scratch healing abilities of H1299 cells overexpressing ASPH were significantly reduced, and protein expression levels decreased. PD03, PD0325901; ASPH, aspartate β-hydroxylase. Scale bars = 200 μm. *$P < 0.05$, **$P < 0.01$, ***$P < 0.001$.

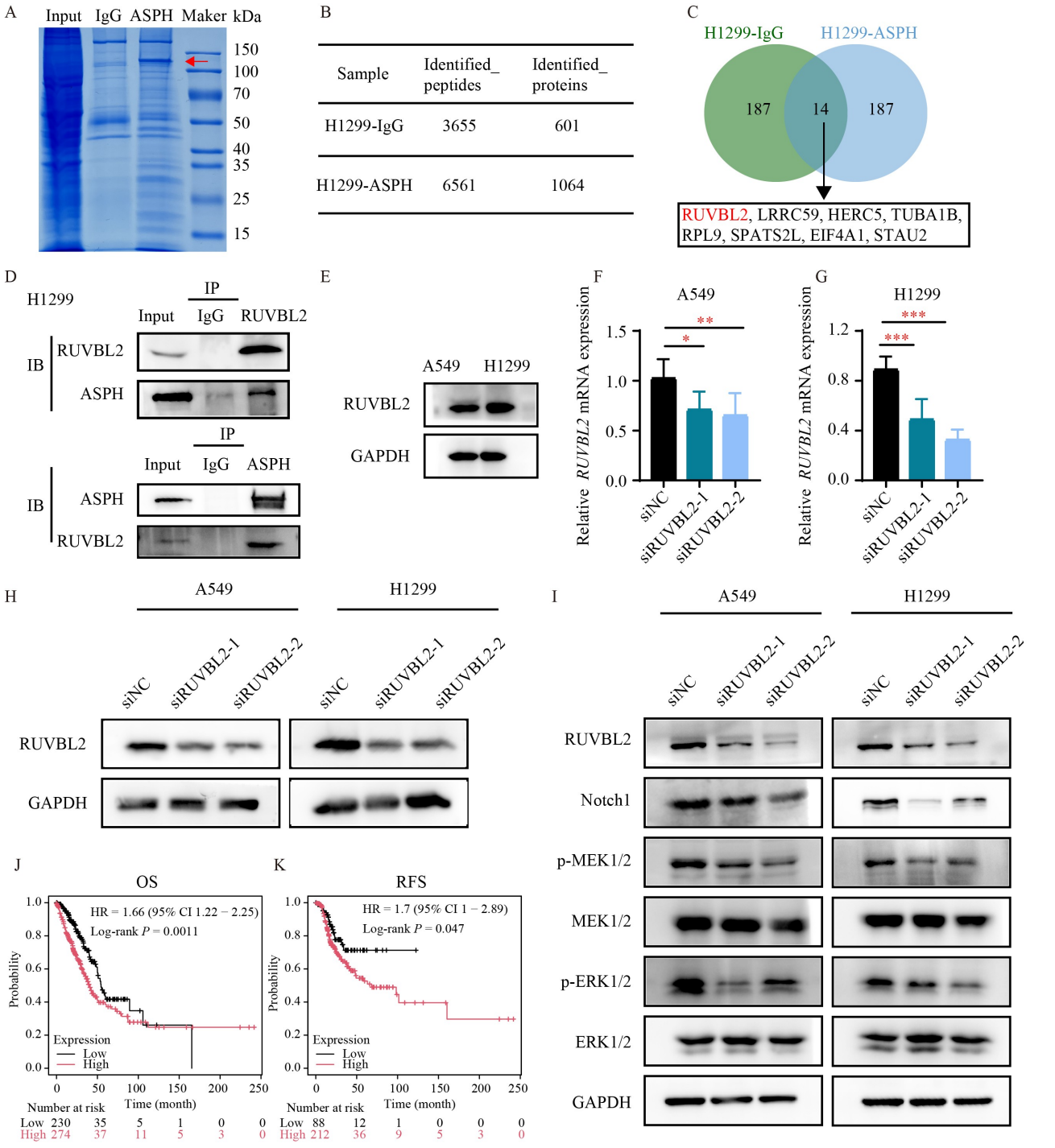

Fig. 5 (A) Coomassie Brilliant Blue staining showing significant enrichment of ASPH protein in H1299 cells overexpressing ASPH pulled down by anti-ASPH antibody. (B) IP-MS results. (C) Venn plots demonstrating the IP-MS results: intersection of 14 differential proteins with protein expression abundance of 0 in the H1299-IgG group and overexpression in the H1299-ASPH group. (D) Co-IP results demonstrating that ASPH interacts with RUVBL2. (E) Western blot assay to detect RUVBL2 expression in LUAD cell lines A549 and H1299. (F–H) RT-qPCR and Western blot assay verified the transfection efficiency of knocking down *RUVBL2* at the mRNA and protein levels, respectively. (I) The results of Western blot assay demonstrated the expression of key molecules of the MAPK signaling pathway and Notch signaling pathway after knocking down *RUVBL2*. (J, K) Kaplan–Meier survival curve analysis of RUVBL2 expression and OS and RFS based on LUAD tissue from the TCGA database. $^{*}P < 0.05$, $^{**}P < 0.01$, $^{***}P < 0.001$. NC, negative control; ASPH, aspartate β-hydroxylase. RUVBL2, RuvB like AAA ATPase 2.

RUVBL2 protein expression levels were significantly reduced in the siRUVBL2-1 and siRUVBL2-2 groups (Fig. 5H).

Further, we detected the altered protein phosphoryla-

tion of key molecules MEK and ERK on MAPK signaling pathway, total protein expression and the expression of key molecule Notch1 on Notch signaling pathway by Western blot assay after knocking down *RUVBL2*, and the results are shown in Fig. 5I, compared with siNC group, after knocking down *RUVBL2*, the key molecules phosphorylated MEK and ERK proteins were reduced, while the total proteins remained unchanged; consistently, Notch1 protein expression was also significantly reduced.

Additionally, by analyzing the relationship between RUVBL2 expression and OS and recurrence-free survival (RFS) in LUAD patients of the TCGA database, we found that patients in the high RUVBL2 expression group had shorter OS and RFS compared to those in the low RUVBL2 expression group. This further confirmed that RUVBL2 expression is significantly positively correlated with poor patient outcomes (HR 1.66, 95% CI 1.22–2.25, $P = 0.001$; HR 1.53, 95% CI 1.00–2.89, $P = 0.047$; Fig. 5J and 5K).

In summary, ASPH promotes LUAD progression by binding to RUVBL2 and activating the MAPK and Notch pathways.

ASPH interacts with RUVBL2 to promote LUAD development

To further validate the relationship between ASPH and RUVBL2, we designed four experimental subgroups: (1) control group: vector + negative control (Vector + siNC); (2) knockdown *RUVBL2* group: vector + knockdown siRUVBL2 group (Vector + siRUVBL2); (3) overexpression ASPH group: ASPH + negative control (ASPH + siNC); (4) Overexpression of ASPH combined with knockdown of *RUVBL2* group: ASPH + siRUVBL*2*.

We first explored the interaction between the two in migration and invasion by Transwell and scratch healing assays and the interaction between the two in MAPK and Notch signaling pathways by Western blot assays. As shown in Fig. 6A–6F, regardless of whether it is in LUAD A549 or H1299 cells, compared with the control group, the number of LUAD cells migrating and invading in the knockdown of *RUVBL2* group was significantly reduced, and the ability of cells to migrate and invade was inhibited. The difference was statistically significant ($P < 0.001$); in the overexpression of ASPH group, the number of cell migration and invasion was significantly increased, and the difference was statistically significant ($P < 0.001$); and compared with the overexpression of ASPH group, the migration and invasion ability of LUAD cells in the overexpression of ASPH combined with the knockdown of *RUVBL2* group was partially inhibited, and the number of cells migrating and invading was close to the level of the control group, and the difference was statistically significant ($P < 0.001$), suggesting that knocking down *RUVBL2* could reverse the pro-migration and invasion effects of ASPH. As shown in Fig. 6G–6J, regardless of whether it is in LUAD A549 or H1299 cells, compared with the control group, knockdown of *RUVBL2* group LUAD cells showed a decrease in scratch healing area and a weakening of healing ability, and the difference between the two groups was statistically significant ($P < 0.001$); overexpression of ASPH group showed an increase in scratch healing area and an enhancement of the healing ability ($P < 0.05$); and the combination of overexpression of ASPH and knockdown of *RUVBL2* group showed a partial inhibition of scratch healing ability ($P < 0.001$), further verifying that knockdown of *RUVBL2* reversed the pro-migratory function of ASPH.

The results of Western blot rescue experiments are shown in Fig. 6K, regardless of whether it is in LUAD A549 or H1299 cells, compared with the NC group, downstream signaling molecules MEK and ERK protein phosphorylation were inhibited and Notch1 expression was weakened in the knockdown of *RUVBL2* group; MEK and ERK protein phosphorylation was activated and Notch1 expression was enhanced in the overexpression of ASPH group; whereas, compared with ASPH overexpression alone, RUVBL2 knockdown in ASPH-overexpressing cells significantly suppressed the phosphorylation levels of MEK and ERK.

In summary, the activation of MAPK signaling pathway by ASPH is dependent on the participation of RUVBL2, and the two may play a cooperative role in promoting LUAD metastasis through protein interactions.

In vivo validation of ASPH promotion of LUAD metastasis

The above results were determined by cell modeling: ASPH and RUVBL2 cooperate with each other may promote LUAD cell metastasis by activating MAPK and Notch signaling pathways. However, whether ASPH still has such a role *in vivo* still needs to be further explored. We first set up two subgroups, i.e., the negative control group shNC and the experimental group shASPH, and infected A549 cells with pLVX-shNC and pLVX-shASPH lentiviruses, respectively, and screened with puromycin to obtain A549 cells that stably knocked down *ASPH*. As shown in Fig. 7A and 7B, we confirmed the infection efficiency of A549-shASPH stably infected cell lines by RT-qPCR and Western blot experiments at the transcriptional and protein levels, respectively, after which we injected these two groups of cells into nude mice via tail vein, respectively, to establish nude mouse lung metastasis model. As shown in Fig. 7D–7F, the number of metastases was significantly reduced in the shASPH group relative to the negative control group, and

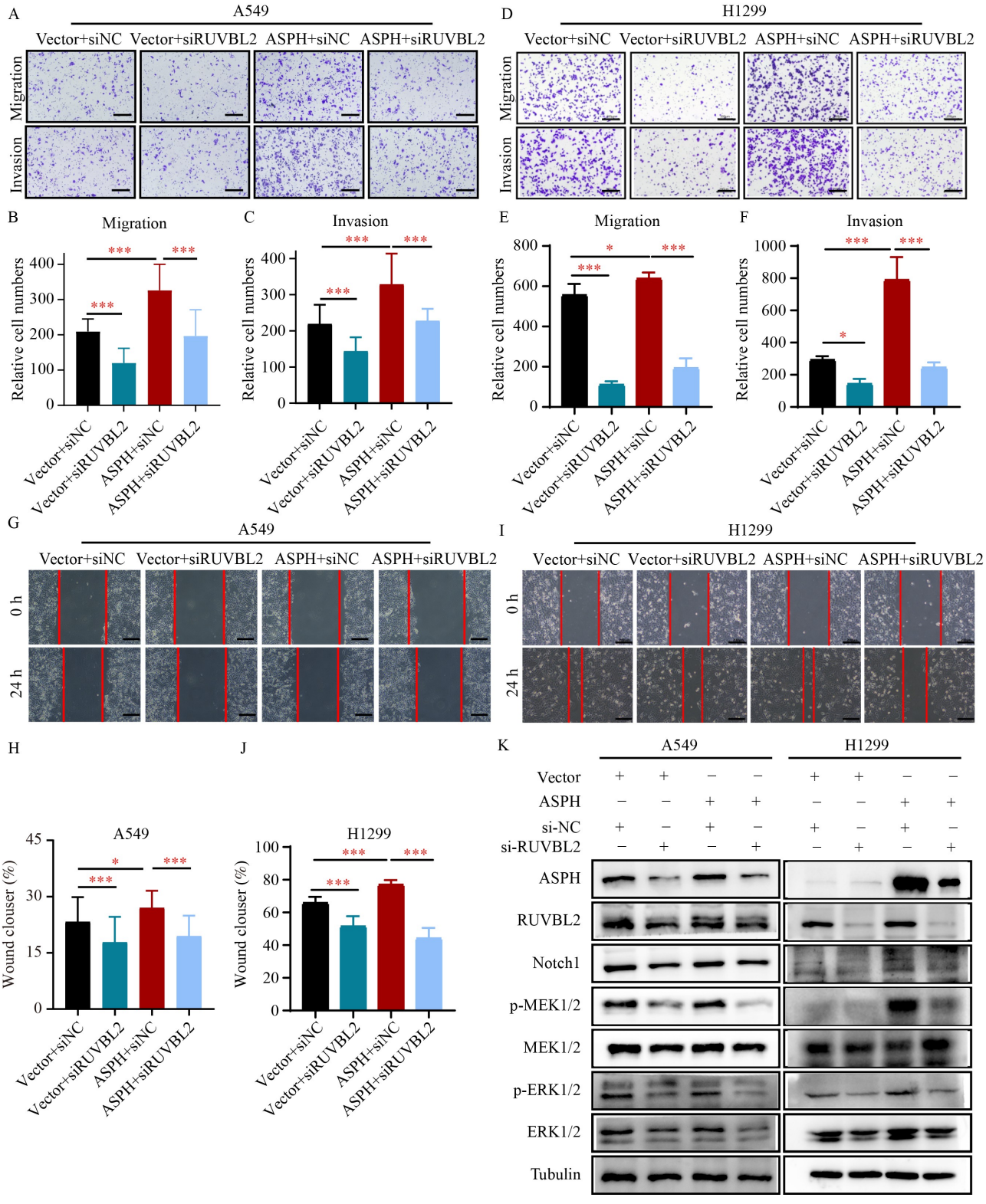

Fig. 6 ASPH interacts with RUVBL2 to promote LUAD development. (A–F) Transwell assays were conducted in A549 and H1299 cells to evaluate the effects of *RUVBL2* knockdown on ASPH-induced LUAD cell migration and invasion. Scale bars = 200 μm. (G–J) Scratch healing assay were conducted in A549 and H1299 cells to evaluate the effects of *RUVBL2* knockdown on ASPH-induced LUAD cell migration. Scale bars = 200 μm. (K) Western blot assays were conducted in A549 and H1299 cells to evaluate the effects of *RUVBL2* knockdown on ASPH-induced MAPK and Notch in LUAD signaling pathways. **P* < 0.05, ****P* < 0.001. NC, negative control; ASPH, aspartate β-hydroxylase; RUVBL2, RuvB like AAA ATPase 2.

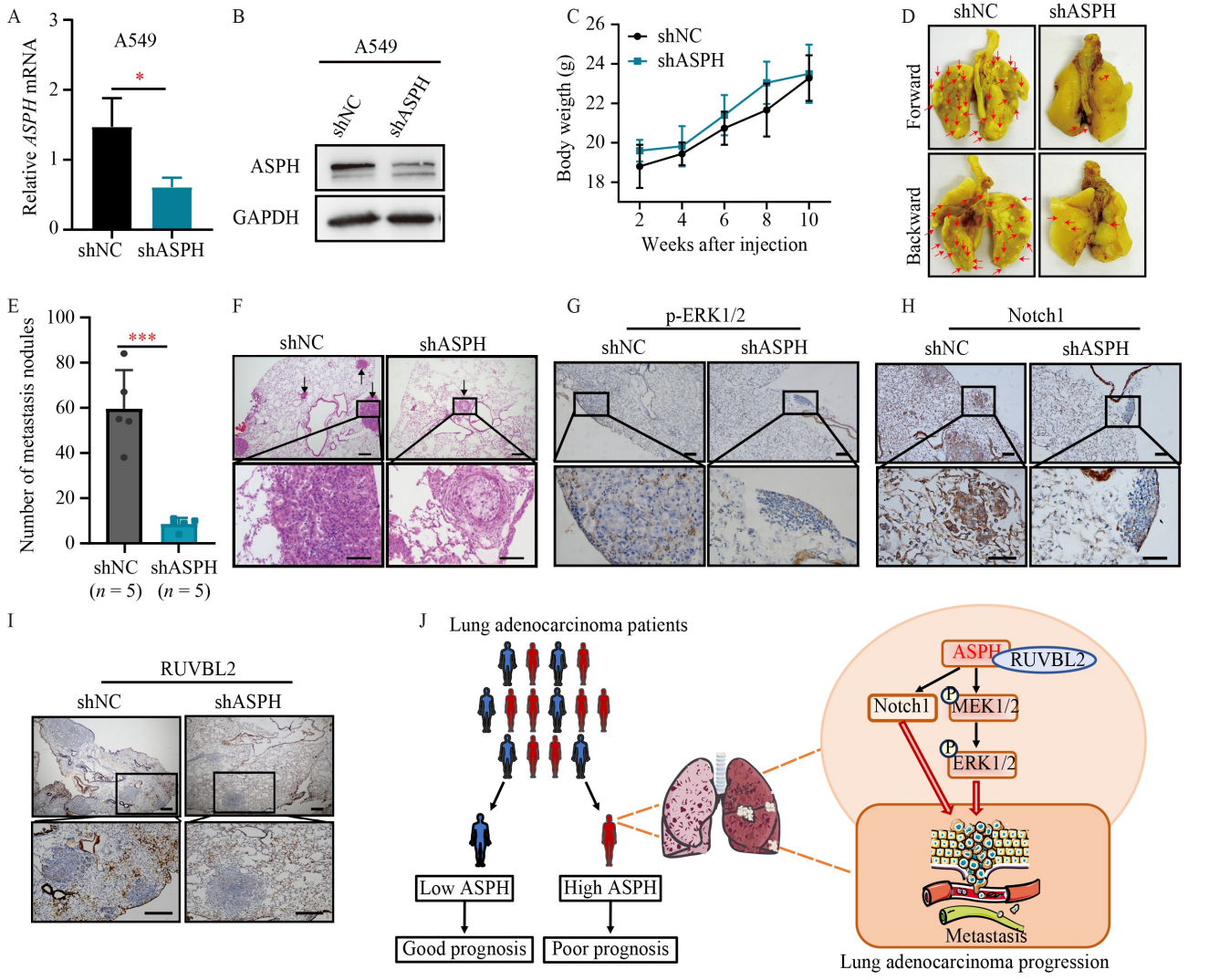

Fig. 7 (A, B) RT-qPCR and Western blot assay to validate the infection efficiency of the lentiviral constructed A549 cell line with stably knocked down *ASPH* for ASPH infection. (C) Mice bodyweight growth folding graph. (D) Grossly representative graphs of two groups of nude mice mouse lung metastasis model. (E) Statistical graphs of the number of lung metastasis. (F) HE staining to detect the effect of ASPH knockdown on the number of metastases in the lungs of two groups of nude mice lung metastasis model. (G, H) IHC staining to detect the effect of *ASPH* knockdown on the expression of key molecules in the pathway. (I) IHC staining to detect the effect of *ASPH* knockdown on the expression of RUVBL2. (J) Schematic diagram of ASPH interacting with RUVBL2 to promote LUAD development by activating MAPK and Notch signaling pathways.

the difference between the two groups was statistically significant (Fig. 7E). Immunohistochemical results showed that the phosphorylation levels of Notch1, a key molecule of the Notch signaling pathway, and ERK, a key molecule of the MAPK signaling pathway, were significantly reduced after knockdown of ASPH (Fig. 7G and 7H). However, we found that after knocking down *ASPH*, there was no significant change in RUVBL2 antigen expression compared to the negative control group (Fig. 7I).

In conclusion, ASPH can promote LUAD cell metastasis through MAPK signaling pathway and Notch signaling pathway *in vivo*.

Discussion

Lung cancer is characterized by a high incidence rate, poor prognosis for patients diagnosed at a late stage, and a high recurrence rate [16]. NSCLC mainly includes LUAD and LUSC, both of which can obtain good survival prognosis in early surgery and treatment, while once metastasis occurs, patients have a poor prognosis [2]. LUAD is mostly peripheral lung cancer, the tumor grows more slowly than squamous carcinoma, but is prone to early distant metastasis and is relatively insensitive to chemotherapy, but responds better to targeted and immunotherapy. Therefore, in the basic research on LUAD, we can improve the survival

prognosis of patients by searching for biomarkers with higher sensitivity and specificity to guide individualized treatment for patients and optimize treatment strategies.

ASPH, also known as aspartate β-hydroxylase (AAH), is a type II transmembrane protein with a molecular weight of approximately 86 kDa, and is a member of the highly conserved α-ketoglutarate-dependent dioxygenase family [17,18]. ASPH is overexpressed in a variety of tumors and the aberrant expression of ASPH is closely associated with a variety of biological responses, such as cell proliferation, migratory invasion, mitochondrial metabolism, and intercellular communication [6,7,10,12,19–25]. Our team found that ASPH is highly expressed in LUAD and is closely related to the survival and prognosis of patients.

In this study, we further demonstrated the differences in *ASPH* expression between LUAD and paraneoplastic normal lung tissues by bioinformatics analysis and clinical samples, and explored the relationship between high ASPH expression and clinicopathologic features by combining TCGA LUAD high-throughput sequencing data and patients' clinical information. Further, we explored the relationship between clinicopathologic features and ASPH expression and OS time of LUAD patients by univariate Cox analysis to identify the prognostic risk factors associated with LUAD; and further explored the independent prognostic risk factors affecting the survival time of LUAD patients by multivariate Cox analysis. The difference between high and low expression of *ASPH* on patients' prognosis was explored by survival curve analysis. ASPH in LUAD is a potential biomarker with diagnostic and prognostic value. In the basic study, we first transfected siRNA or ASPH overexpression plasmid, and determined the transfection efficiency of knockdown or overexpression of *ASPH* by RT-qPCR and protein immunoblotting experiments. Then cell function experiments were performed, and in LUAD cells, we determined the biological functions of ASPH to promote migration and invasion by Transwell and scratch experiments. To further explore the biological mechanisms by which ASPH exerts its functions, we performed differential gene pathway enrichment analysis based on ASPH expression differences on TCGA-LUAD high-throughput sequencing data, and found that ASPH expression-associated differential genes were significantly enriched in the PI3K-Akt and MAPK signaling pathways, and in view of the fact that the Notch pathway is more widely reported in other types of cancers, we analyzed these three different genes via protein immunoblotting experiments to validate the expression of key molecules on these three pathways after knockdown and overexpression of *ASPH*. We found that MAPK and Notch signaling pathways were significantly inhibited after *ASPH* knockdown, while the pathways were activated after overexpression of ASPH. However, the PI3K-Akt signaling pathway was not changed by ASPH. To further explore the mechanism of ASPH action, we performed immunoprecipitation combined with mass spectrometry analysis to identify the interaction of RUVBL2 with ASPH.

RUVBL2, also known as Reptin, is a member of the conserved ATPase (AAA +) superfamily associated with cellular activity, and together with RuvB-like protein 1, RNA polymerase II-associated protein 3, and Hsp90 1 structural domain-interacting protein 1, it forms the R2TP (Rvb1-Rvb2-Tah1-Pih1, R2TP) complex, which is involved in assembly, activation or maturation of macromolecular complexes of phosphatidylinositol-3-kinase-like family of kinases (PIKKs) such as mTORC1 [26,27]. RUVBL2 is involved in cell survival, cell differentiation, immune microenvironment, and other biological processes critical for biological processes critical for tumorigenesis and development [28–34]. In colon cancer, RUVBL2 has been reported to have a positive feedback effect with YTHDF1, which promotes colon cancer development through the MAPK signaling pathway [35]. We hypothesized that there might be a synergistic effect between ASPH and RUVBL2, and subsequently verified the interactions between ASPH and RUVBL2 by protein immunoprecipitation experiments, and the functional responses of Transwell, scratch assay, and protein immunoblotting experiments confirmed that ASPH combined with RUVBL2 exerted its biological function of promoting metastasis in LUAD and promoted metastasis through the activation of MAPK and Notch signaling pathways. Finally, we constructed a lung metastasis model in nude mice to validate the metastasis-promoting function of ASPH *in vivo*.

Interestingly, we observed that *RUVBL2* knockdown led to a simultaneous reduction in both ASPH mRNA and protein levels, suggesting that RUVBL2 may regulate ASPH expression primarily at the transcriptional level. This finding does not exclude the possibility that downstream signaling pathways modulated by RUVBL2 might further influence ASPH transcription. Although the detailed mechanism remains to be clarified, this adds another layer of complexity to the RUVBL2-ASPH regulatory axis and warrants further investigation.

Overall, our results confirm that ASPH is a prognostic marker for LUAD and plays an important pro-cancer role in LUAD, and our experimental results provide a potential therapeutic targets for LUAD patients. Although the results of the present study help to improve the understanding of the relationship between ASPH and LUAD and the related molecular mechanisms, certain limitations remain. First, whether there is a direct correlation between ASPH and RUVBL2 protein still needs to be proved; second, the specific regulatory mechanism of ASPH on MAPK signaling pathway failed to be thoroughly investigated; and third, the *in vivo*

backfill experiment of knocking down *RUVBL2* on LUADs with high expression of ASPH still needs to be thoroughly investigated in the future.

Conclusions

In conclusion, our study demonstrated that ASPH is highly expressed in lung adenocarcinoma and that high ASPH expression positively correlates with aggressive clinicopathological characteristics, which predicts poor clinical prognosis of LUAD patients and may serve as an independent risk factor for predicting the prognosis of LUAD. ASPH promotes LUAD progression through activation of MAPK and Notch signaling pathways by RUVBL2. This may provide a new promising target for LUAD treatment.

Acknowledgements

The authors acknowledge the contribution of all investigators at the participating study sites. This study was supported in part by the grant from Guangdong Basic and Applied Basic Research Fund (2023A1515110995).

Compliance with ethics guidelines

Conflicts of interest Chuhong Huang, Huihao Lu, Jiali Dong, Yanming Lin, Yuting Chen, Zhixiong Yang, Wenmei Su, and Zhen Cheng declare that they have no conflict of interest.

The study was approved by the Ethics Committee of the Affiliated Hospital of Guangdong Medical University (Approval No. YJKT2025-030-1) and the study was performed in accordance with the ethical standards as laid down in the 1964 Declaration of Helsinki and its later amendments or comparable ethical standards. Informed consent was obtained from all patients for being included in the study.

Data availability and compliance statement

The authors declare that the acquisition and subsequent use of all data presented in this manuscript comply fully with all relevant local, national, and international laws, regulations, ethical guidelines, and the terms of use associated with the original data sources.

The authors bear full legal responsibility for ensuring the legality of data acquisition and all subsequent uses.

The data that support the findings of this study are available on request from the corresponding author.

Electronic supplementary material Supplementary material is available in the online version of this article at https://doi.org/10.1007/s11684-025-1182-y and is accessible for authorized users.

References

1. Siegel RL, Kratzer TB, Giaquinto AN, Sung H, Jemal A. Cancer statistics, 2025. CA Cancer J Clin 2025; 75(1): 10–45
2. Hendriks LEL, Remon J, Faivre-Finn C, Garassino MC, Heymach JV, Kerr KM, Tan DSW, Veronesi G, Reck M. Non-small-cell lung cancer. Nat Rev Dis Primers 2024; 10(1): 71
3. Lancet T, 0. Lung cancer treatment: 20 years of progress. Lancet 2024; 403(10445): 2663
4. Zeng H, Ran X, An L, Zheng R, Zhang S, Ji JS, Zhang Y, Chen W, Wei W, He J. Disparities in stage at diagnosis for five common cancers in China: a multicentre, hospital-based, observational study. Lancet Public Health 2021; 6(12): e877–e887
5. Kanwal M, Smahel M, Olsen M, Smahelova J, Tachezy R. Aspartate β-hydroxylase as a target for cancer therapy. J Exp Clin Cancer Res 2020; 39(1): 163
6. Zou Q, Hou Y, Wang H, Wang K, Xing X, Xia Y, Wan X, Li J, Jiao B, Liu J, Huang A, Wu D, Xiang H, Pawlik TM, Wang H, Lau WY, Wang Y, Shen F. Hydroxylase activity of ASPH promotes hepatocellular carcinoma metastasis through epithelial-to-mesenchymal transition pathway. EBioMedicine 2018; 31: 287–298
7. Lin Q, Chen X, Meng F, Ogawa K, Li M, Song R, Zhang S, Zhang Z, Kong X, Xu Q, He F, Bai X, Sun B, Hung MC, Liu L, Wands J, Dong X. ASPH-notch axis guided exosomal delivery of prometastatic secretome renders breast cancer multi-organ metastasis. Mol Cancer 2019; 18(1): 156
8. Ogawa K, Lin Q, Li L, Bai X, Chen X, Chen H, Kong R, Wang Y, Zhu H, He F, Xu Q, Liu L, Li M, Zhang S, Nagaoka K, Carlson R, Safran H, Charpentier K, Sun B, Wands J, Dong X. Aspartate β-hydroxylase promotes pancreatic ductal adenocarcinoma metastasis through activation of SRC signaling pathway. J Hematol Oncol 2019; 12(1): 144
9. Barboro P, Benelli R, Tosetti F, Costa D, Capaia M, Astigiano S, Venè R, Poggi A, Ferrari N. Aspartate β-hydroxylase targeting in castration-resistant prostate cancer modulates the NOTCH/HIF1α/GSK3β crosstalk. Carcinogenesis 2020; 41(9): 1246–1252
10. Peng H, Guo Q, Xiao Y, Su T, Jiang TJ, Guo LJ, Wang M. ASPH regulates osteogenic differentiation and cellular senescence of BMSCs. Front Cell Dev Biol 2020; 8: 872
11. Nagaoka K, Ogawa K, Ji C, Cao KY, Bai X, Mulla J, Cheng Z, Wands JR, Huang CK. Targeting aspartate beta-hydroxylase with the small molecule inhibitor MO-I-1182 suppresses cholangiocarcinoma metastasis. Dig Dis Sci 2021; 66(4): 1080–1089
12. Zhou Q, Lin J, Yan Y, Meng S, Liao H, Chen R, He G, Zhu Y, He C, Mao K, Wang J, Zhang J, Zhou Z, Xiao Z. INPP5F translocates into cytoplasm and interacts with ASPH to promote tumor growth in hepatocellular carcinoma. J Exp Clin Cancer Res 2022; 41(1): 13
13. Gan X, Li S, Wang Y, Du H, Hu Y, Xing X, Cheng X, Yan Y, Li Z. Aspartate β-hydroxylase serves as a prognostic biomarker for neoadjuvant chemotherapy in gastric cancer. Int J Mol Sci 2023; 24(6): 5482
14. Zhu H, Liu H, Wen J, Yuan T, Ren G, Jiang Y, Yuan Y, Mei J, Yu Y, Li G. Overexpression of human aspartyl (asparaginyl) β-

hydroxylase in NSCLC: its diagnostic value by means of exosomes of bronchoalveolar lavage. Appl Immunohistochem Mol Morphol 2021; 29(10): 720–727
15. Győrffy B. Integrated analysis of public datasets for the discovery and validation of survival-associated genes in solid tumors. Innovation 2024; 5(3): 100625
16. Siegel RL, Miller KD, Wagle NS, Jemal A. Cancer statistics, 2023. CA Cancer J Clin 2023; 73(1): 17–48
17. Stenflo J, Ohlin AK, Owen WG, Schneider WJ. beta-Hydroxyaspartic acid or beta-hydroxyasparagine in bovine low density lipoprotein receptor and in bovine thrombomodulin. J Biol Chem 1988; 263(1): 21–24
18. Stenflo J, Holme E, Lindstedt S, Chandramouli N, Huang LH, Tam JP, Merrifield RB. Hydroxylation of aspartic acid in domains homologous to the epidermal growth factor precursor is catalyzed by a 2-oxoglutarate-dependent dioxygenase. Proc Natl Acad Sci USA 1989; 86(2): 444–447
19. Yao WF, Liu JW, Huang DS. MiR-200a inhibits cell proliferation and EMT by down-regulating the ASPH expression levels and affecting ERK and PI3K/Akt pathways in human hepatoma cells. Am J Transl Res 2018; 10(4): 1117–1130
20. Xu L, Ma Y, Zhang H, Lu QJ, Yang L, Jiang GN, Liao WL. HMGA2 regulates circular RNA ASPH to promote tumor growth in lung adenocarcinoma. Cell Death Dis 2020; 11(7): 593
21. Xu Y, Kang P, Leng K, Yao Y, Liao G, Han Y, Shi G, Zhong X, Cui Y. Circ_ASPH promotes cholangiocarcinoma growth and metastasis through the miR-581/ATP-binding cassette transporter G1 signaling pathway. Cancer Commun (Lond) 2020; 40(10): 545–550
22. Holtzman NG, Lebowitz MS, Koka R, Baer MR, Malhotra K, Shahlaee A, Ghanbari HA, Bentzen SM, Emadi A. Aspartate β-hydroxylase (ASPH) expression in acute myeloid leukemia: a potential novel therapeutic target. Front Oncol 2021; 11: 783744
23. Xiao M, Chen X, Chen W, Wang L, Rao X, Luo C. Overexpression of ASPH protein predicts poor outcomes in retroperitoneal liposarcoma patients. Chin Med J (Engl) 2023; 136(17): 2113–2115
24. Zhang Y, Guo J, Zhang L, Li Y, Sheng K, Zhang Y, Liu L, Gong W, Guo K. CircASPH enhances exosomal STING to facilitate M2 macrophage polarization in colorectal cancer. Inflamm Bowel Dis 2023; 29(12): 1941–1956
25. Cao X, Yang J, He L, Liu C. Circ_0005699 Expedites ox-LDL-Triggered Endothelial Cell Injury via Targeting miR-384/ASPH Axis. Cardiovasc Toxicol 2024; 24(10): 1067–1076
26. Rodríguez CF, Llorca O. RPAP3 C-terminal domain: a conserved domain for the assembly of R2TP Co-Chaperone Complexes. Cells 2020; 9(5): 1139
27. Mao YQ, Seraphim TV, Wan Y, Wu R, Coyaud E, Bin Munim M, Mollica A, Laurent E, Babu M, Mennella V, Raught B, Houry WA. DPCD is a regulator of R2TP in ciliogenesis initiation through Akt signaling. Cell Rep 2024; 43(2): 113713
28. Flavin P, Redmond A, McBryan J, Cocchiglia S, Tibbitts P, Fahy-Browne P, Kay E, Treumann A, Perrem K, McIlroy M, Hill ADK, Young LS. RuvBl2 cooperates with Ets2 to transcriptionally regulate hTERT in colon cancer. FEBS Lett 2011; 585(15): 2537–2544
29. Kim SG, Hoffman GR, Poulogiannis G, Buel GR, Jang YJ, Lee KW, Kim BY, Erikson RL, Cantley LC, Choo AY, Blenis J. Metabolic stress controls mTORC1 lysosomal localization and dimerization by regulating the TTT-RUVBL1/2 complex. Mol Cell 2013; 49(1): 172–185
30. Anne-Aurélie R, Joaquim J, Osman B, Véronique N, Jean R. Reptin regulates insulin-stimulated Akt phosphorylation in hepatocellular carcinoma via the regulation of SHP-1/PTPN6. Cell Biochem Funct 2017; 35(6): 289–295
31. Joaquim J, Nathalie AC, Nicolas S, Pierre C, Capucine H, Fadila B, Rémi P, Corinne B, Nestor PL, Marcio DC, Catherine P, Daniela C, Pierre D, Jean R, Samira BT. Liver Reptin/RUVBL2 controls glucose and lipid metabolism with opposite actions on mTORC1 and mTORC2 signalling. Gut 2017; 67(12): 2192–2203
32. Yenerall P, Das AK, Wang S, Kollipara RK, Li LS, Villalobos P, Flaming J, Lin YF, Huffman K, Timmons BC, Gilbreath C, Sonavane R, Kinch LN, Rodriguez-Canales J, Moran C, Behrens C, Hirasawa M, Takata T, Murakami R, Iwanaga K, Chen BPC, Grishin NV, Raj GV, Wistuba II, Minna JD, Kittler R. RUVBL1/RUVBL2 ATPase activity drives PAQosome maturation, DNA replication and radioresistance in lung cancer. Cell Chem Biol 2020; 27(1): 105–121.e14
33. Jie T, Mingxin W, Peng G, Maoxiao F, Guangwei W. RUVBL1 ubiquitination by DTL promotes RUVBL1/2-β-catenin-mediated transcriptional regulation of NHEJ pathway and enhances radiation resistance in breast cancer. Cell Death Dis 2024; 15(4): 259
34. Wang Z, Yang C, Wang X, Liao H, Liu X, Liu H, Zhang M, Zhang L, Wang H. Knockdown of RUVBL2 improves hnRNPA2/B1-stress granules dynamics to inhibit perioperative neurocognitive disorders in aged mild cognitive impairment rats. Aging Cell 2025; 24(3): e14418
35. Chen D, Ji F, Zhou Q, Cheung H, Pan Y, Lau HCH, Liang C, Yang Z, Huang P, Wei Q, Cheung AHK, Kang W, Chen H, Yu J, Wong CC. RUVBL1/2 blockade targets YTHDF1 activity to suppress m6A-dependent oncogenic translation and colorectal tumorigenesis. Cancer Res 2024; 84(17): 2856–2872